



Full-scale SPH simulations of ship-wave impact generated sea spray

Shafiu Mintu ^{*}, David Molyneux, Bruce Colbourne

Department of Ocean & Naval Architectural Engineering, Memorial University of Newfoundland, St. John's, NL, A1B 3X5, Canada

ARTICLE INFO

Keywords:

Sea spray
Smooth particle hydrodynamics (SPH)
Ship-wave impact
Green water
DualSPHysics
Multi-phase simulation
Ice accretion

ABSTRACT

Sea spray generated by ship-wave impact contributes to marine ice accretion onboard vessels. Limitations in field measurements and model experiments encourage the use of numerical simulation to understand the formation of such spray. In this paper, full-scale computational fluid dynamics (CFD) models of wave-generated sea spray are developed using a smooth particle hydrodynamics (SPH) method. A three-dimensional (3D) numerical wave tank equipped with a flap-type wave maker and a wave absorber is created to produce regular waves of various heights and steepness. A full-scale medium-size fishing vessel (MFV) is modeled to encounter incoming waves at head sea conditions at various forward speeds. Moving ship dynamics with three degree-of-freedom (3-DOF) in waves are resolved instead of mimicking a relative ship speed. The resultant spray water amount is measured using a numerical collection box and compared against field measurements and a theoretical model, where a reasonable agreement is found. The model is able to distinguish between green water and spray water. A multi-phase two-dimensional (2D) simulation is also performed that demonstrates the role of winds in the fragmentation of water sheets into droplets. The simulation results indicate energy released from a surging ship significantly contributes to the generation of spray.

1. Introduction

Vessels and offshore structures operating in cold climates are subject to ice accretion. Wave-impact spray generation is the dominant source of marine icing and contributes to between 50% and 90% of the icing on ships (Zakrzewski, 1986a; Zakrzewski et al., 1988). The remaining amount comes from atmospheric sources, depending on the geographic locations (Mintu et al., 2016). The mechanism of ship-generated spray due to wave impacts is not yet fully understood (Horjen, 2013; Kulyakhtin and Tsarau, 2014; Lozowski et al., 2000; Shipilova et al., 2012; Zakrzewski et al., 1988). At present, it can only be postulated (Bodaghkhani et al., 2016) by identifying possible mechanisms published in the literature. The first postulation is that spray forms directly at the time of impact by splashing resulting from the ship interaction with the wave crest due to ship motion (Jones and Andreas, 2012; Zakrzewski, 1986b). The second postulation describes the formation of spray in multiple steps. First, a jet or sheet of water rises above the ocean surface along the hull of the ship as the moving bow encounters a wave as shown in Fig. 1. Second, the water sheet breaks into ligaments, and the ligaments further break to form droplets under wind action, similar to the production of spume droplets (Dehghani et al., 2017; Ryerson, 2013; Zakrzewski et al., 1988).

The local impact velocity of the wave particles, air entrainment, surrounding wind velocities, and the motions of the ship determine the ejection velocity and the thickness of the water sheets. This high-velocity water sheet cannot remain unbroken (Ryerson, 2013). How, when, and where at the ship bow the sheet breakup occurs is not yet well predicted. Wind plays a vital role in the generation of droplets for both natural spray and wave-impact-generated spray. A critical wind speed in the range of 8–19 m/s is required to produce spray droplets (Andreas, 1990; Horjen, 2013; Horjen and Vefsnmo, 1985; Jones and Andreas, 2012). The droplet diameter of the spray cloud can vary from very fine, at 14 µm, to very large, at 7.7 mm (Ryerson, 1995), similar in characteristic size to jet and spume droplets (Mintu et al., 2019). After ejection, the droplets interact with the airflow, exchanging momentum, heat, and moisture with the surrounding air (Veron, 2015) and form layers of ice in favorable conditions.

Discretizing the governing equations for very fine water droplets over a very large domain in the size scale of a vessel makes numerical simulations of spray very challenging. Fragmentation and large reconstruction of breaking free surface create numerical instability for grid-based computational fluid dynamics (CFD) due to mesh overlapping and domain distortion (Domínguez et al., 2019; Kanehira et al., 2020; Zha et al., 2021). Smooth Particle Hydrodynamics (SPH) - a meshless

* Corresponding author.

E-mail address: shafiu.mintu@mun.ca (S. Mintu).

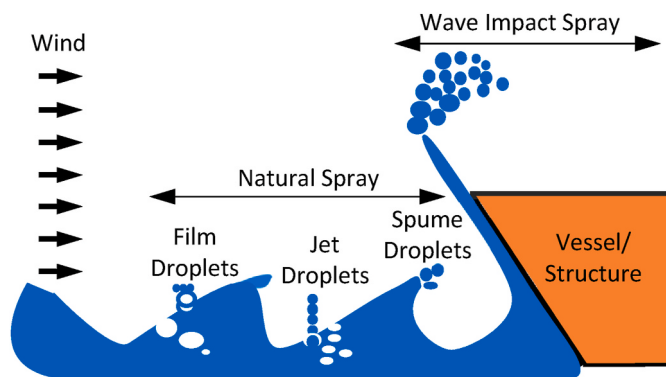


Fig. 1. Sketch of the sea spray cloud formation.

Lagrangian particle-based method is a widely validated and accepted method for solving violent flows (Kanehira et al., 2020; Kawamura et al., 2016; Roselli et al., 2019; Shadloo et al., 2016; Zha et al., 2021). The method can avoid numerical diffusion and the governing equation is free of convective terms, hence avoid numerical errors that can be seen in Eulerian methods (Kanehira et al., 2020). There are two types of SPH methods: Weakly compressible SPH (WCSPH) and Incompressible SPH (ISPH) methods. The difference between the two methods is their treatment of the pressure term in the governing equation. The WCSPH utilizes equation of state to compute pressure, where ISPH solves a system of linear equations in each time step which makes ISPH more accurate and stable than WCSPH. On the flip side, for a real-world application with a large number of particles, ISPH is computationally expensive (Akbari, 2018).

WCSPH-based open-source CFD solver DualSPHysics (Crespo et al., 2015) has been successfully employed by many researchers to study violent free surfaces (Altomare et al., 2020; Kanehira et al., 2020; Kawamura et al., 2016; Roselli et al., 2019; Tagliafierro et al., 2021). Green water shipping onboard a vessel was simulated and validated against model scale experiments by Kawamura et al. (2016). Two different size domains were created, one for transient motion in the following sea and the other for the periodic steady-state in the stern quarter sea. Water depth was reduced to one-third, shifted from deep water to shallow water, for the quarter sea to accommodate the limitation of computing resources. Short crested and multi-directional waves in a circular basin were modeled by Kanehira et al. (2020), where a reasonable agreement was reported against the model scale experimental data. Waves with lower frequencies and steepness were better predicted than the higher frequency and steeper waves. Finer resolution of the domain with a larger number of particles or adaptive resolution was suggested to improve very high-frequency waves.

Roselli et al. (2019) simulated the surf-zone originating from wave breaking and run-up on sloped beaches in shallow water based on DualSPHysics solver. Validation against experimental data showed that the wave breaking kinematics were well captured. The maximum errors in the wave crests and troughs were found after wave splash-up, where fragmentation of the free surface occurred. Air entrainment in the experiment was identified as a possible factor that was not modeled, limiting the accuracy of the simulation. A multi-phase solver was recommended to improve the prediction. A full-scale SPH simulation of a wave impacting a large pier in a sea storm was simulated by Altomare et al. (2020). The water surface elevation and velocity field were extracted from the 2D simulations and applied as a forcing boundary condition in the 3D simulations, eliminating the requirements for a very large domain for the waves to fully develop. Domínguez et al. (2013) also demonstrated a full-scale SPH simulation of wave impacting an oil rig with a large fluid domain of 170 m × 114 m × 68 m. A particle spacing of 6 cm generated more than 1 billion particles and was computed on 64 GPUs [Tesla M2090] for almost a week.

Most of the numerical simulations of water spray, green water, or breaking wave in the past studies were conducted in model scale; either in 2D (Roselli et al., 2019) or 3D (Kawamura et al., 2016; Silva et al., 2017; Z. Wang et al., 2016). Full-scale 3D simulations were carried out primarily for resistance and self-propulsion and were validated against model scale data (Begovic et al., 2020) or other potential flow models (Tezdogan et al., 2016). Most 3D models use zero forward speed of the ship (only heave and pitch) in the simulation (Greco et al., 2013), or prescribed motions extracted from model experiments (Silva et al., 2017) to minimize the domain size.

Appropriate scaling of spray properties (surface tension, impact pressure) and measurements in model scale experiments remains a challenge (Chung et al., 1998; Sapone, 1990). While scaled physical experiments are valid for qualitative assessments, they are questionable for quantitative analysis of spray cloud. Full-scale measurements are more reliable in this respect, even though full scale measurements are complex and limited by measurement uncertainties since the experiments cannot be done in controlled environments. Although theoretical models give a quick estimate of the spray properties, they often lack modeling all aspects of the spray physics. Numerical simulation can offer an integrated approach where multiple physical elements can be modeled properly and overcome the limitations of scaled model experiments and field measurements. Theoretical and empirical models together with numerical models can give a broader understanding of the dynamic nature of the spray physics.

Simulation of spray events involves a range of physics processes: wave breaking, air entrapment, break-up of water sheets and droplets, de-coupling spray water from green water, and finally distributions of resultant droplets over the deck. Reproducing all these physics elements in an integrated numerical simulation, therefore, is challenging. The multi-scale nature of this problem also makes simulation computationally expensive. However, different stages of the spray process can be modeled separately. To the best of the authors' knowledge, wave-generated spray for ships in full-scale has never been simulated. Very recently, Tagliafierro et al. (2021) simulated whisker spray generated by a high-speed planing hull at Froude number (Fr) 1.443 in calm water using DualSPHysics. No quantitative validation was presented, only a qualitative depiction of the spray was discussed. In this paper, the open-source code DualSPHysics version 5.0 was utilized to simulate full-scale wave-generated sea spray. The paper is organized as follows: first, the choice of available spray measurement data for validation studies is discussed in the next section. Next, the SPH method and the various SPH techniques that were employed are discussed. The simulation results are then presented and compared against a Russian field measurement (Zakrzewski, 1986b) and a theoretical model previously published by the authors (Mintu et al., 2021). Finally, the paper concludes with future recommendations.

2. Sea spray data

The limited data available for ship-wave impact generated spray falls into two categories: (1) scale model experiments (Chung et al., 1998; Sapone, 1990) and (2) full-scale field measurements (Borisov and Pchelko, 1975; Horjen et al., 1986; Panov, 1976; Ryerson, 1995; Thomas, 1991). For water spray, model scale results are not reliable due to inappropriate scaling of the real phenomenon. Even though (Sapone, 1990) introduced the most sophisticated approach to scale down the critical spray properties, the water's Weber number (ratio of inertia to surface tension forces) was still 22 times smaller than the full-scale requirement (Mintu et al., 2021). Scaling up the amount of water to full-scale would give an unrealistic and questionable value. Some simplified experiments on wave run up against a vertical wall in model scale (Bodaghkhani et al., 2016) and in full-scale (Aalbers and Poen, 2015) were reported, but they are not representative of the dynamic nature of ship-wave interactions. Among the three studies of full-scale spray generation available in the literature as reported by Samuels

Table 1
Principal particulars of MFV Narva.

Parameters	Target Values	Achieved	References
LOA (m)	39.5	39.6	Zakrzewski et al. (1988)
LBP (m)	N/A	36.0	
Beam (m)	7.3	7.3	
Draft (m)	3.0	3.0	
Freeboard (m)	3.5	3.5	Samuelson et al. (2017)
Stem angle (deg)	70	70	Dehghani et al. (2016b)
Contour of the bulwark	$X = 0.5457Y^2$	$X = 0.5457Y^2$	Zakrzewski et al. (1988)
Displacement (tonne)	462	402.55	Zakrzewski (1989)

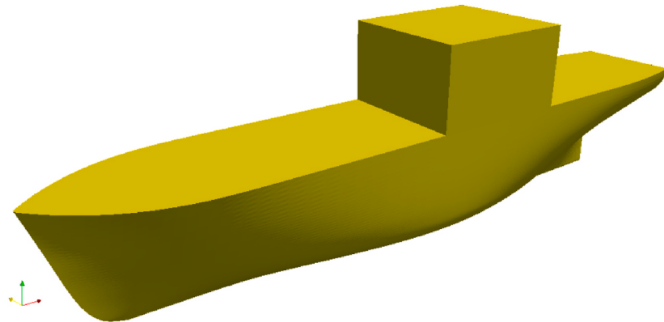


Fig. 2. 3D CAD model of MFV Narva.

et al. (2017), data from a 39 m Russian fishing boat “MFV Narva” (Borisenkov and Pchelko, 1975) were selected for validation in this study due to their completeness. This data was also used by many researchers as a benchmark data for spray generation (Dehghani et al., 2016a; Kulyakhtin and Tsarau, 2014; Lozowski et al., 2000; Samuelson et al., 2017; Shipilova et al., 2012). The data were retrieved and compiled by Zakrzewski (1986a, 1986b) from a soviet icing database and expressed in an empirical formula. How the spray property was measured is, however, unknown.

The amount of water that falls on a deck for a single impact event is described by spray flux (Samuelson et al., 2017; Zakrzewski, 1986b) as

$$F_s = EV_d l_{wc} t_{dur} \text{ kg/m}^2 \quad (1)$$

where E is the collection or collision efficiency of the droplets, V_d is the droplet velocity (assumed to be equal to local relative wind speed), t_{dur} is the duration of the spray event, and l_{wc} is the liquid water content of the spray measured at the field measurements of (Borisenkov and Pchelko, 1975) and expressed as

$$l_{wc} = 24.2 \times \exp(-0.55Z) \text{ g/m}^3 \quad (2)$$

where Z is the elevation above the deck of the MFV.

This empirical formula was further generalized by Zakrzewski (1986b) and later by Mintu et al. (2021), respectively as follows:

$$l_{wc} = 6.36e^{-5} H_s V_r^2 \cdot \exp(-0.55(z - 3.5)) \text{ kg/m}^3 \quad (3)$$

$$l_{wc} = 4.69e^{-10} E_T \cdot \exp(-0.55(z - 3.5)) \text{ kg/m}^3 \quad (4)$$

where H_s is the significant wave height, V_r is the ship velocity relative to the wave, E_T is the total energy released by a single ship-wave impact, z is elevation from the sea level instead of from the deck after Samuelson et al. (2017).

The total amount of spray water was calculated assuming the spray flux was coming through the “window” of 10 m height and breadth equal to the beam of the vessel as reported by Zakrzewski (1986a).

Previous numerical simulation (Mintu et al., 2019) and theoretical model (Dehghani et al., 2016a) indicate this “window” assumption is reasonable.

For the ship model of MFV Nava, no lines plan was available in the literature. Based on the available data spread out in multiple references as summarized in Table 1, the hull geometry of Narva was estimated using DelftSHIP and Rhino CAD software. Special attention was given to match the bow shape (bulwark contour and stem angle). A 3D CAD model is shown in Fig. 2, and the lines plan is given in the appendix in Fig. 22.

3. SPH method

3.1. Governing equations

SPH is a mesh-less, fully Lagrangian method (Gingold and Monaghan, 1977), where the grids are completely abandoned and the continuum is represented by a set of material points known as particles. Particles are geometrical positions in the continuum that carry physical properties such as volume, mass, momentum, temperature, concentration, or other hydrodynamic properties (Shadloo et al., 2016). The differential form of the Navier-Stokes equations is transformed into particle summations by discrete approximations. The continuity equation (Eq. (5)) and momentum conservation equations of weakly compressible fluid for water (Eq. (6)) and for air (Eq. (7)) (Mokos et al., 2015) are described by

$$\frac{dp}{dt} = -\rho \nabla \cdot u \quad (5)$$

$$\frac{du}{dt} = -\frac{\nabla P}{\rho_w} + g + \nu_0 \nabla^2 u + \frac{1}{\rho_w} \nabla \cdot \vec{\tau} \quad (6)$$

$$\frac{du}{dt} = \frac{\nabla P}{\rho_a} + g + \frac{1}{\rho_a} (\nabla \cdot \rho_a \nu_0 \nabla) u \quad (7)$$

where ρ is the fluid density, ρ_w indicates water density while ρ_a is air density, u is the velocity vector, P is the pressure, g is the gravitational acceleration, ν_0 is the laminar kinematic viscosity, and $\vec{\tau}$ is the large eddy simulation Sub-Particle Scale (SPS) stress tensor (Dalrymple and Rogers, 2006). The pressure P can be directly computed from the equation of state (Batchelor, 1967; Monaghan et al., 1999) for single and multi-phase flow respectively as

$$P(\rho) = B \left[\left(\frac{\rho}{\rho_0} \right)^{\gamma} - 1 \right] \quad (8)$$

$$P(\rho) = B \left[\left(\frac{\rho}{\rho_0} \right)^{\gamma} - 1 \right] + X - a\rho^2 \quad (9)$$

where the coefficient $B = C_s^2 \rho_0 / \gamma$ is constant for each phase, C_s is the speed of sound, ρ_0 is the initial density of the fluid, and γ is the isentropic expansion factor. The inclusion of the -1 term in the equation of state allows automatic capturing of free surface behavior and fragmentation (Pereira et al., 2018). The term X signifies a constant background pressure and the term $a\rho^2$ prevents the dispersion of the air into the water and the subsequent fragmentation of the interface (Mokos et al., 2015), where a is a cohesion factor defined as

$$a = 1.5g(\rho_{0w} / \rho_{0a})L \quad (10)$$

where ρ_{0w} and ρ_{0a} are the initial densities of the water and air respectively and L is the characteristic length scale of the problem being modeled.

3.2. Discretization of governing equations

The derivatives of the governing equations are estimated at any point

in space using a kernel approximation, which is analogous to finite difference and finite volume discretization techniques in mesh-based CFD. The principle is to approximate any function F by the integral approximation

$$F(r) = \int_{\Omega} F(r') W(r - r', h) dr' \quad (11)$$

where W is the kernel function, r is the position vector, h is the smoothing length that is the influencing area of the kernel function, Ω is the interpolation domain, and the symbol denotes an approximation.

In discrete SPH, equation (11) is further approximated using the interpolant formula and called particle approximation (Z.-B. Wang et al., 2016).

$$F(r_i) = \sum_{j=1}^N F(r_j) W(r_i - r_j, h) \frac{m_j}{\rho_j} \quad (12)$$

where N is the total number of particles in the calculation region.

In SPH notation, equations (5)–(7) can be discretized respectively after Dalrymple and Rogers (2006) as

$$\frac{d\rho_i}{dt} = \rho_i \sum_j \left[(u_i - u_j) \cdot \nabla_i W_i \frac{m_j}{\rho_j} \right] + \mathfrak{D}_t \quad (13)$$

$$\frac{du_i}{dt} = - \sum_j m_j \left(\frac{P_i + P_j}{\rho_i \cdot \rho_j} \right) \nabla_i W_{ij} + g + \sum_j m_j \left(\frac{4\nu_0 r_{ij} \cdot \nabla_i W_{ij}}{(\rho_i + \rho_j)(r_{ij}^2 + \eta^2)} \right) u_{ij} + \sum_j m_i \left(\frac{\bar{\tau}_{ab}^{ij}}{\rho_j^2} + \frac{\bar{\tau}_{ab}^{ji}}{\rho_i^2} \right) \nabla_i W_{ij} \quad (14)$$

$$\frac{du_i}{dt} = - \sum m_j \left(\frac{P_i + P_j}{\rho_i \cdot \rho_j} + \Pi_{ij} \right) \nabla_i W_{ij} - 2a\rho_a^2 \sum_j \frac{m_j}{\rho_j} \nabla_i W_{ij} + g \quad (15)$$

where t is time, $r_{ij} = r_i - r_j$ is particle position, $u_{ij} = u_i - u_j$ is particle velocity, P_i and P_j are pressure, ρ_i and ρ_j are density, m_i and m_j are mass, the subscripts i and j represent particles i and j , ρ_a is the density of air, $g = (0, 0, -9.81) \text{ ms}^{-2}$ is the gravitational acceleration, ν_0 is the laminar kinematic viscosity, $\bar{\tau}_{ab}$ is the SPS stress tensor, $\eta^2 = 0.01 h^2$, and W_{ij} is the kernel function that depends on the distance between particles i and j (Altomare et al., 2017).

The density diffusion term \mathfrak{D}_t modified by Fourtakas et al. (2020) with a coefficient of 0.1 as recommended by (Altomare et al., 2020; Kanehira et al., 2020) was applied to improve the pressure field in the wave basin. The stability, accuracy, and speed of SPH simulation depends on the choice of the smoothing kernel distribution as well as the smoothing length (Shadloo et al., 2016). In this work, the Quintic (Wendland, 1995) kernel was used. Wendland kernel circumvents clustering of neighboring particles due to the onset of the tensile instability (Zha et al., 2021) and is widely used (Altomare et al., 2020; Kanehira et al., 2020; Kawamura et al., 2016). It is expressed as

$$W(r, h) = \frac{7}{4\pi h^3} \left(1 - \frac{q}{2} \right)^4 (2q + 1) \quad 0 \leq q \leq 2 \quad (16)$$

where $q = \frac{r}{h}$, r is the distance between any two given particles i and j , and h is the smoothing length.

The artificial viscosity term Π_{ij} is used to resolve numerical instability and is given by

$$\Pi_{ij} = \begin{cases} -\alpha \bar{c}_{ij} \mu_{ij} & u_{ij} \cdot r_{ij} < 0 \\ 0 & u_{ij} \cdot r_{ij} > 0 \end{cases} \quad (17)$$

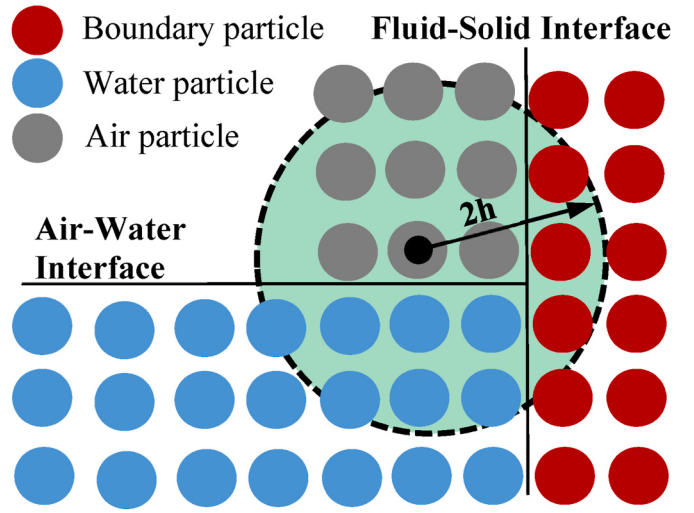


Fig. 3. Sketch of different types of particles, interfaces, and dynamic boundary condition.

where α is a coefficient that needs to be tuned in order to introduce

realistic dissipation (Altomare et al., 2015), $\bar{c}_{ij} = \frac{c_i + c_j}{2}$ is the mean speed of sound, μ_{ij} is the kinematic viscosity given by

$$\mu_{ij} = \frac{h \cdot u_{ij} \cdot r_{ij}}{r_{ij}^2 + 0.01h^2} \quad (18)$$

where $r_{ij} = (r_i - r_j)$ and $u_{ij} = (u_i - u_j)$ are the particle position and velocity respectively and h is the smoothing length.

3.3. Boundary conditions

A dynamic boundary condition (DBC) (Crespo et al., 2015) was applied to the flap-type wave paddle, bottom of the wave basin, and the ship model. In DBC, the solid boundaries are modeled using boundary particles that differ from the fluid particles. The fluid particles experience a repulsion force when close to the boundary particles at a distance smaller than twice the smoothing length (h) as illustrated in Fig. 3. The incoming fluid particles cause the density of the affected boundary particles to increase according to Eq. (13), resulting in a pressure increase as per Eq. (8) for water and Eq. (9) for air. The consequence is an increase in the pressure term $((P_i + P_j)/\rho_i \cdot \rho_j)$ in the momentum equation (Eq. (14) for water and Eq. (15) for air), which leads to a repulsive force being exerted on the fluid particle. In the case of air-water flow, the interface between water particles and air particles is modeled by the Colagrossi and Landrini multi-phase model (Mokos et al., 2015). The advantage of DBC is that it can be applied to any arbitrary 2D and 3D geometries at a low computational cost. The boundary particles were set to a no-slip condition.

The size of the domain for this study was selected considering several objectives: (1) to minimize wave reflection, (2) to minimize wave decay during long simulations as reported by Kanehira et al. (2020), and (3) to make the domain long enough for the moving ship to encounter at least one wave at the highest speed. Different sizes of wave basins with different types of wave generators (piston vs flap) fitted with dissipative

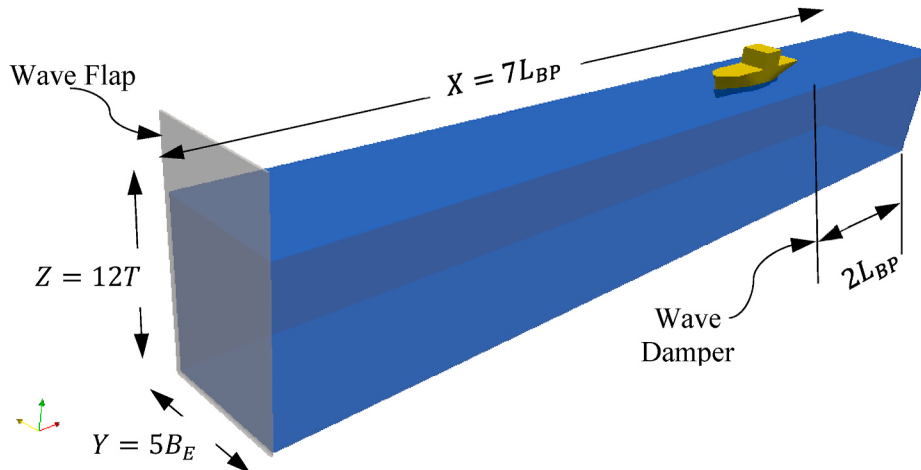


Fig. 4. Full-scale numerical wave basin with a flap-type wave maker and a numerical wave damper.

beach or numerical wave absorber at the end of the tank were examined. The domain that demonstrated the best characteristics in terms of accuracy and computational time was selected and is shown in Fig. 4. The motion of the wave paddle was assigned by a time-dependent input file to generate the target waves. The ship was modeled as a rigid floating object which moves at a desired forward speed with the ability to heave and pitch freely. The other motions were restricted. The ship stops at $2L_{BP}$ from the wave maker, fulfilling ITTC recommendation for inlet boundary condition to avoid any wave reflection. The side walls of the tank were modeled as open boundaries with no physical walls (Gomez-Gesteira et al., 2012), therefore no friction. The walls were spaced apart by five times the effective beam of the vessel for head sea encounter, a standard size width also used by (Kawamura et al., 2016; Tagliafierro et al., 2021). A numerical wave damper was installed at the end of the tank to cancel out wave reflections (Crespo et al., 2015). Various depths were examined to finalize an optimal depth that fulfills deep water wave criteria.

It was observed in the simulation that the DBC created a non-physical gap between the incoming water and ship's boundary as reported by (Kanehira et al., 2020; Mokos et al., 2016). To counter this numerical effect, a particle shifting technique with a default shifting coefficient was applied. A particle shifting algorithm proposed by Vacondio et al. (2013) for weakly compressible SPH model was used in this study. The particle shifting distance δr_s is given by

$$\delta r_s = -D \nabla C_i \quad (19)$$

where D is a diffusion coefficient and C_i is the particle concentration calculated as

$$D = AhU_i dt \quad (20)$$

where A is a dimensionless constant and a proposed value of 2 was used (Akbari, 2019), U_i is the local particle velocity, and dt is the current time step.

$$\nabla C_i = \sum_j \frac{m_j}{\rho_j} \nabla W_{ij} \quad (21)$$

A free surface correction that limits diffusion to the surface normal but allows shifting on the tangent to the free surface was employed to avoid a truncated-kernel error and the consequent non-physical instabilities as reported by Zha et al. (2021).

3.4. SPH parameters

A non-dimensional smoothing length of $h/dp = 1.7$ was used as recommended by (Altomare et al., 2017; Kanehira et al., 2020). Here, h

Table 2
Selected regular wave parameters.

Wave ID	Wave Height, Hs [m]	Wave Period [s]	Ship length to Wavelength [L/λ]	Steepness [Hs/λ]
3W1	3	6.80	0.55	1/24
6W2	6	6.80	0.55	1/12
6W3	6	5.66	0.80	1/8.33
6W4	6	5.06	1.00	1/6.65
6W7	6	6.00	0.70	1/9.35
6W8	6	4.60	1.20	1/5.5

is the smoothing length and dp is the particle resolution. A second order accurate explicit time integrator called simplistic scheme was employed with a variable time step after (Kanehira et al., 2020; Roselli et al., 2019). This scheme also works better for high-frequency impacts expected in this study [DualSPHysics guide v4.2]. A laminar SPS viscosity scheme with a kinematic viscosity of water of $10^{-6} \text{ m}^2/\text{s}$ was employed to treat the viscous dissipation of momentum.

3.5. Numerical collection box

A numerical collection box of the same size of the "window" (10 m height and breadth equal to the beam of the vessel) and length equal to a few ship lengths was placed just above the deck to capture the spraying water. The "flowtool" function of DualSPHysics code was utilized for this purpose. The box captures the number of particles that go in and out of the pre-defined boundary. It also computes the average velocity of the particles. The volume of the water is calculated by multiplying the volume of one particle by the total number of particles. With the velocity of the particles, the flow rate also can be calculated.

An NVIDIA Tesla T4 GPU (Graphics Processing Unit) was used to run the simulations. A GPU is proven to be faster and cheaper than multi-core CPU workstations (Mintu and Molyneux, 2018).

4. Results and discussion

4.1. Wave generation

Wave characteristics were not recorded during the field measurements of (Borisenkov and Pchelko, 1975; Panov, 1976), but were later recovered by Zakrzewski (1986a, 1986b) based on the fetch duration reported by the former authors. As per their report, regular waves of two different heights and various ship lengths to wavelength ratios (L/λ) were generated as tabulated in Table 2. The default wave generation function for the flap-type wavemaker of DualSPHysics was not able to

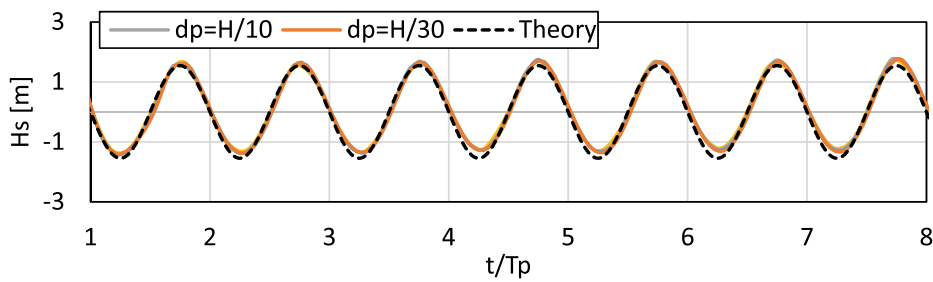


Fig. 5. Comparison of numerical and theoretical wave elevation at various particle resolutions for 3W1.

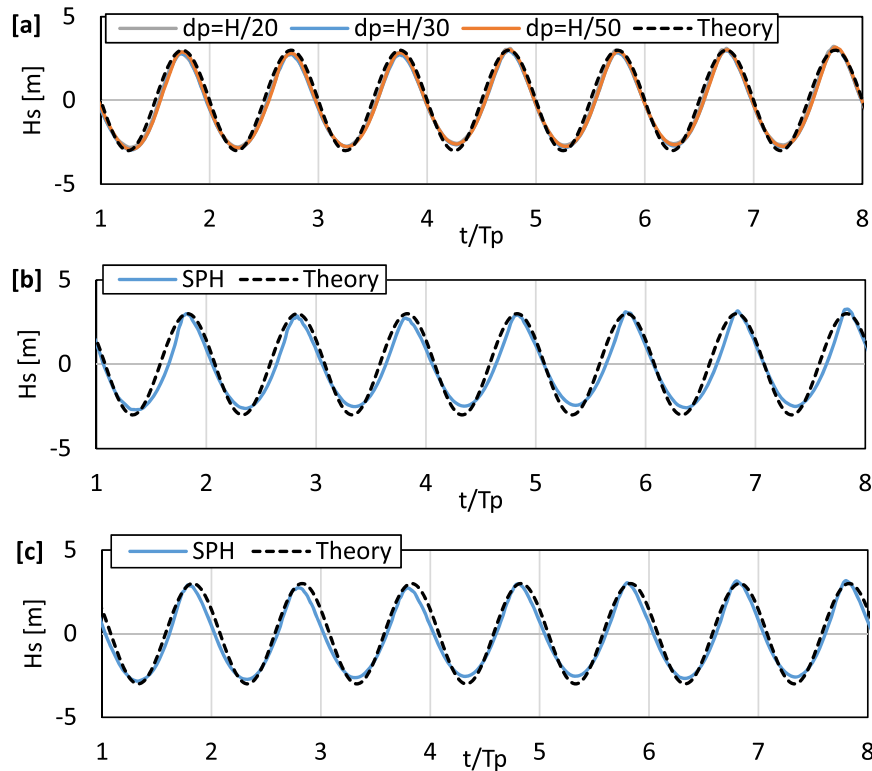


Fig. 6. Comparison of numerical and theoretical wave elevation at various particle resolutions for [a] 6W2, [b] 6W3, [c] 6W7.

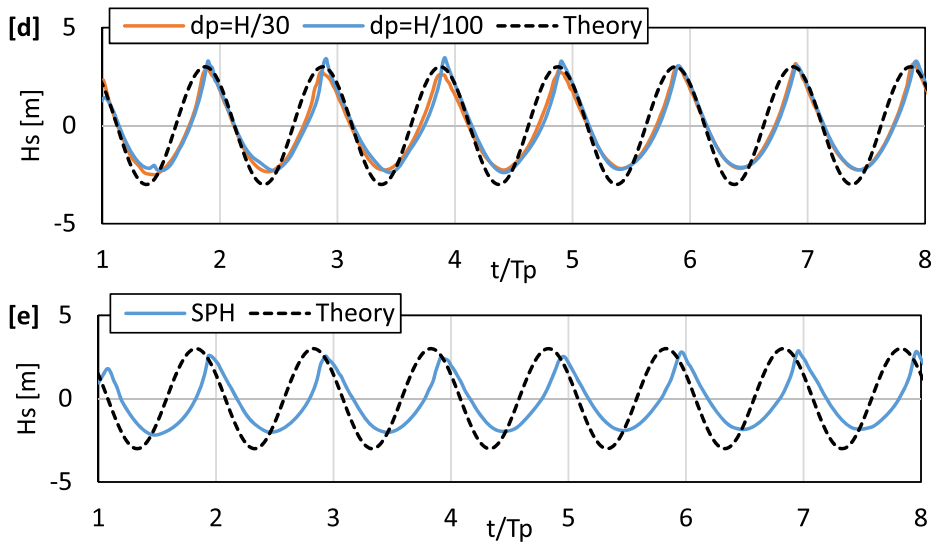


Fig. 7. Comparison of numerical and theoretical wave elevation for steeper waves [d] 6W4, [e] 6W8.

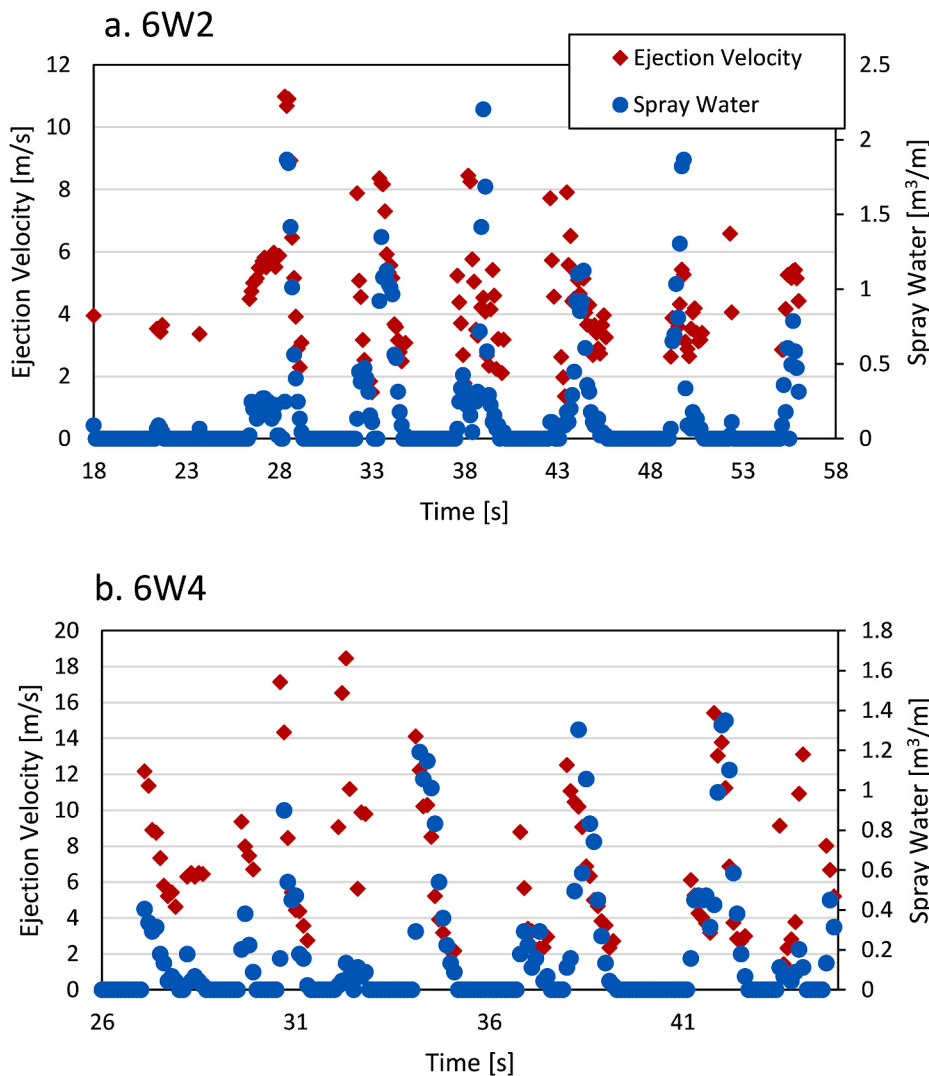


Fig. 8. Numerical estimation of ejection velocity and volume of spray water in 2D simulation for waves a) 6W2, b) 6W4, at Fr 0.156.

produce the desired waves accurately. Therefore, a new wave generation function was implemented. The movement of the flap for deep water was calculated and imposed as an external boundary motion. It is found that for $dp = H/10$, longer waves (3W1, 6W2, 6W3, and 6W7) were produced very accurately (within 5% error margin) as shown in Fig. 5 and Fig. 6. This dp resolution is also recommended by Altomare et al. (2017). However, for the higher frequency, steeper waves (6W4 and 6W8), a larger error margin was evident when compared with the linear wave theory (see Fig. 7).

4.2. 2D spray simulation

It was realized early in the study that the generation of spray in a simulated environment would be challenging. At zero forward speed with various encounter frequencies, it was found that the boat simply reacted to the incoming wave almost in-phase and resulted in some green water but no sign of spray generation. It was recognized that a surge motion along with heave and pitch with a certain phase difference between waves and ship motions are required to produce spray within the limited size of the wave basin. The timing of the collision between waves and the moving ship is therefore important.

Table 3
Selected ship speed and waves for 3D simulations.

Froude number [Fr]	3W1	6W2	6W3	6W4	6W7	6W8
0.0			X			
0.144		X				
0.156			X			
0.222		X				
0.480			X	X	X	X

Two-dimensional (2D) simulations were performed first to fine-tune the spray generation, by changing the phase difference between the waves and ship motion. The ship was kept stationary until the wave was fully developed. After four to five wave cycles, the ship was allowed to move forward at various designated speeds of Fr 0.156 and 0.222. The ship was allowed to pitch and heave in addition to surge, while roll, sway, and yaw motions were restricted. Fig. 8 shows the ejection velocity and volume of spray water for each wave impact for Fr 0.156. In addition to visual inspection, a spray ejection velocity threshold was used to distinguish between spray water and green water as defined by Mintu et al. (2021). Any spray ejection speed below the threshold was

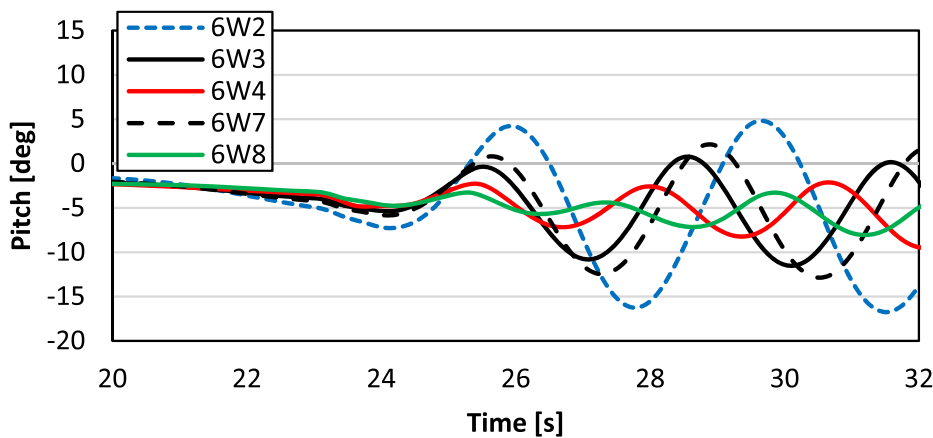


Fig. 9. Time history of ship pitch motions for various waves at Fr 0.48.

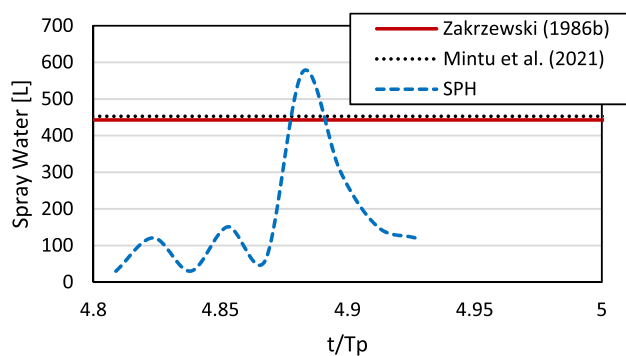


Fig. 10. Time distribution of amount of spray water for 3W1 at Fr 0.222.

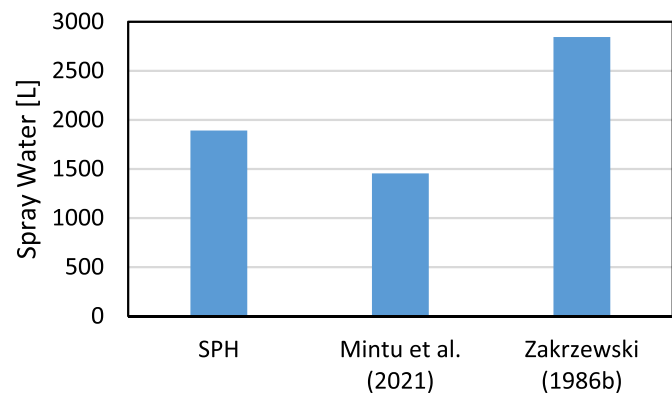


Fig. 12. Comparison of the amount of spray water for 6W2 at Fr 0.48.

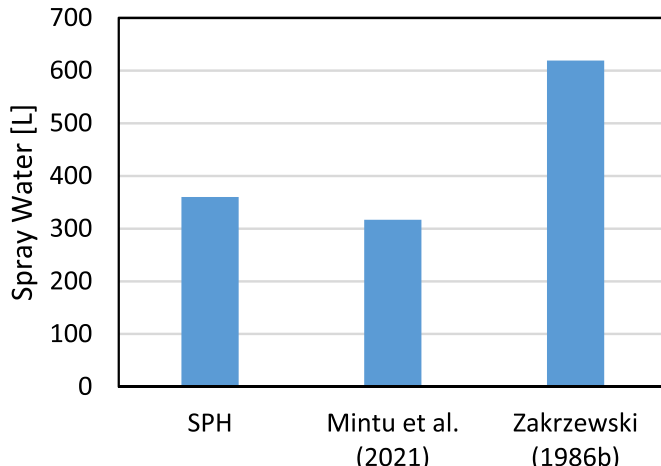


Fig. 11. Comparison of the amount of spray water for 6W2 at Fr 0.156.

considered green water. The spray velocity threshold was calculated by $\sqrt{2gF_{br}}$, where F_{br} is the freeboard relative to wave. For a wave height of 3 m and 6 m, the threshold velocity can be found approximately 6 m/s and 3.5 m/s, respectively.

For wave 6W2, the wavelength was too long compared to the ship

length ($L/\lambda = 0.55$). As a result, excessive pitch motion caused green water shipping. Only spray events occurred at 28.7 s and 37.9 s. With an $L/\lambda = 1$, wave 6W4 created the cleanest spray events more frequently than the rest.

4.3. 3D spray simulation

Although 2D simulations produced spray events, they are not reliable when the end goal is to estimate the amount of water. The boundary shape of the bow in 3D has a varying stem and flare angles that cannot be captured in a 2D simulation. A 3D simulation is therefore desirable. Experience from the 2D simulation guided the selection of the combination of waves and ship speed (Fr) for a 3D simulation as outlined in Table 3.

Fr 0.144, 0.156, and 0.222 came from the reported field measurements (Borisenkov and Pchelko, 1975; Panov, 1976). A calculated Fr of 0.48 was found to be an ideal speed to achieve the desired encounter frequency as reported by Sapone (1990) to minimize the pitch motion of the vessel. As the waves get steeper, the pitch motion becomes smaller as shown in Fig. 9. This was necessary to decouple spray events from the excessive deck wetness or green water event that were experienced at lower Froude numbers. In addition, the ship required less time to travel the wave basin, which in turn optimized simulation run time. All the simulations were run at head sea condition (180° relative wave direction). For 3D simulation, the finest possible resolution of $H/30$ was used,

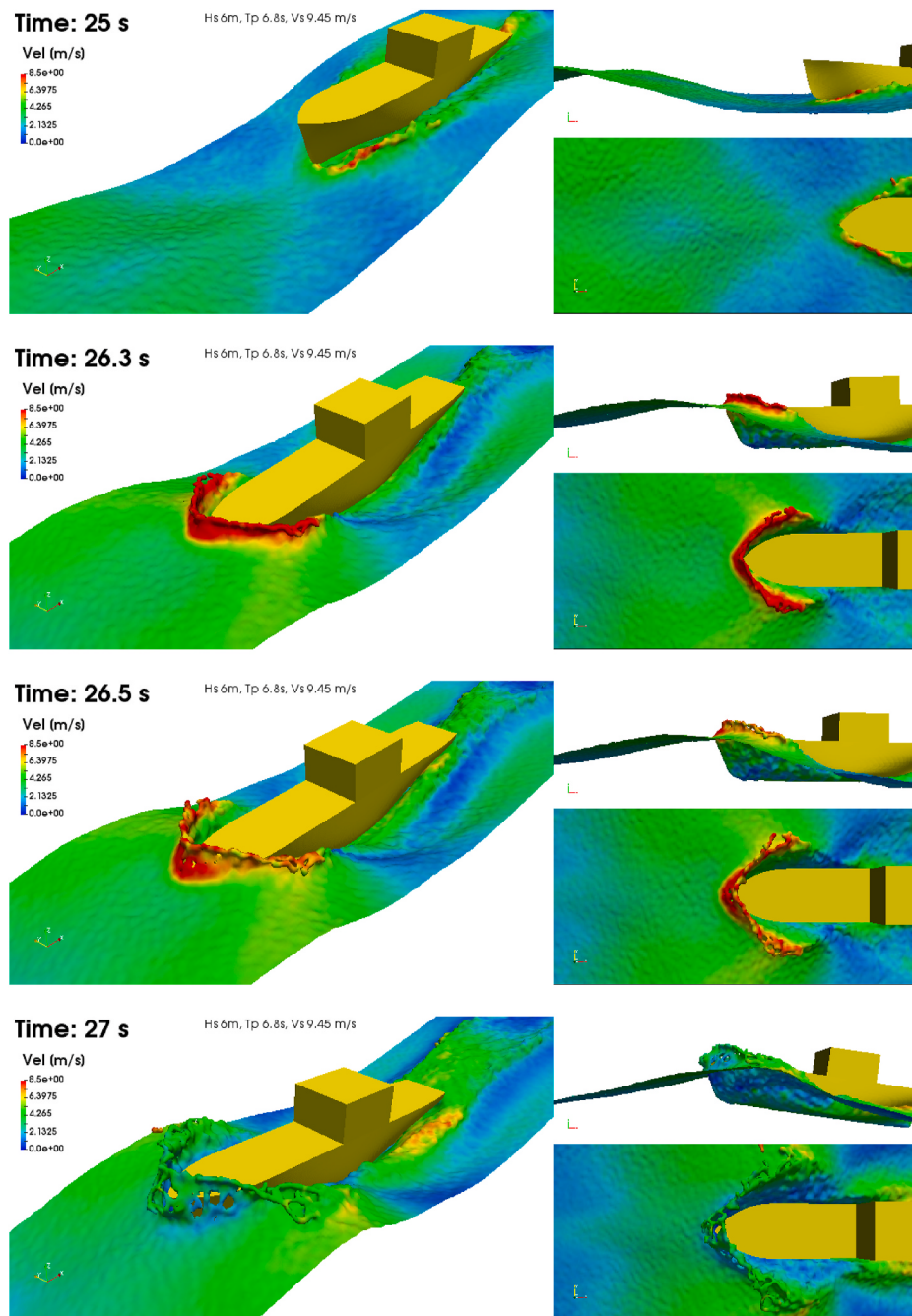


Fig. 13. Development of ship-wave impact generated spray over time for wave 6W2 at Fr 0.48.

Table 4
Comparison of estimated spray water for various waves and Froude number.

Wave ID	Fr	Spray Water [L]		
		SPH	Mintu et al. (2021)	Zakrzewski (1986b)
6W2	0.156	359.90	316.61	618.73
6W2	0.48	1891.47	1454.38	2844.34
6W7	0.48	1339.45	956.88	1871.46
6W3	0.48	1034.15	903.64	1767.36
6W4	0.48	879.12	813.40	1590.93
6W8	0.48	666.74	747.44	1461.94

which created more than 35 million particles and took 95 h (~4 days) to simulate 56 seconds of physical time. Simulation beyond this resolution was not possible due to the memory limit of the available GPU.

Even though field measurements reported spray, for wave 3W1 at Fr 0.144 the simulation did not produce any spray for this condition. The ship's speed was found to be too low for a relatively long and gentle wave. To determine the amount of spray water, the following steps were adopted for each case. First, time histories of spray water and their ejection velocities were plotted and the spray threshold was used to isolate spray water events from green water events. Second, the time average value of the selected spray water was calculated by integrating the spray event. Fig. 10 shows the distribution of spray water over time for wave 3W1 at Fr 0.222. The higher bound of this distribution is in reasonable agreement with the field measurement and theoretical model. For the steeper wave 6W2, the SPH predictions are reasonable with the theoretical model, while the empirical formula gave the higher bounds as shown in Fig. 11 and Fig. 12. Fig. 13 shows the development of the spray at various time steps for 6W2 at Fr 0.48. Table 4 summarizes

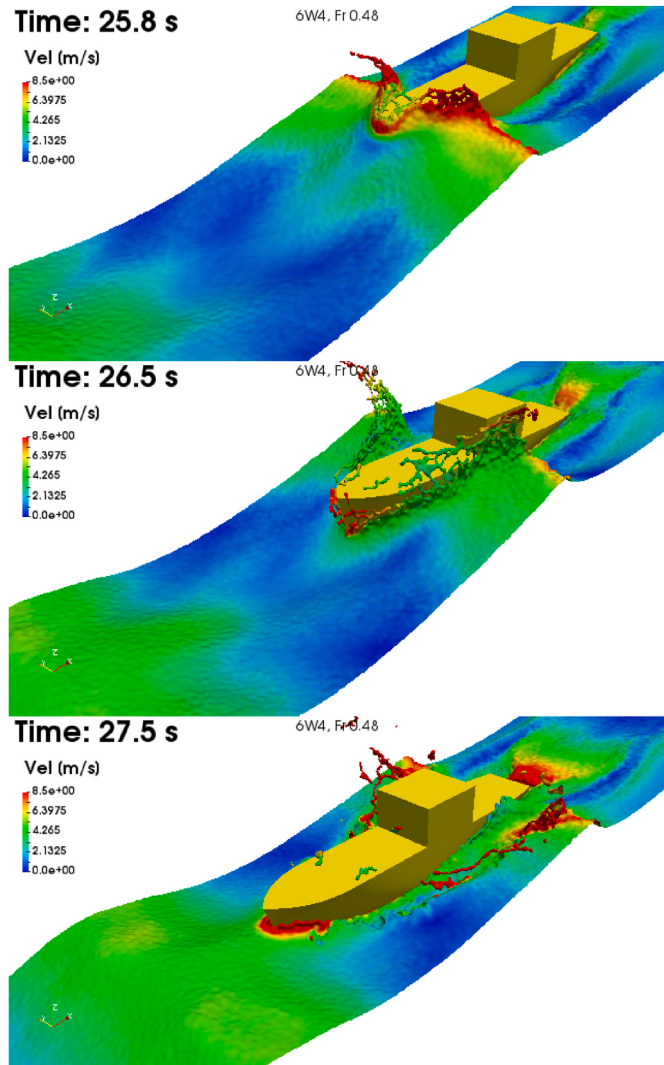


Fig. 14. Development of sea spray in wave 6W4 at Fr 0.48. A video showing the development of the spray is provided in the supplemental material.

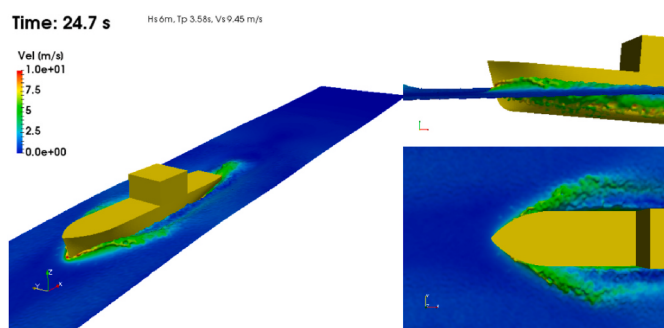


Fig. 15. Bow wave in calm water.

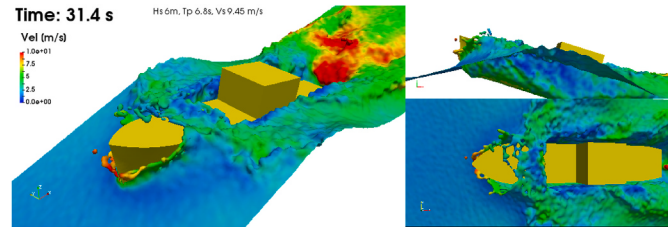


Fig. 16. Green water loading for 6W2 at Fr 0.48. (For interpretation of the references to colour in this figure legend, the reader is referred to the web version of this article.)

the amount of spray water for all cases and compares it with theoretical and empirical models.

Wave 6W4 with $L/\lambda = 1$ produced the cleanest spray among all the simulations both in 2D as well as in 3D. This scenario produced an enormous amount of spray water at the bow at the time of impact, but most of the spray deflected out of the deck over time and only a fraction of it ended up on the deck as shown in Fig. 14. The final outcome on the amount of spray water onboard, therefore, largely depends on the incident wind speed and direction. Due to the current limitations of multi-phase simulations in 3D (more descriptions in section 4.4), the current study assumes that the amount of sea spray at the time of generation is dominated by the wave impact. Wind will contribute to producing finer droplets only.

Comparing the liquid film breakup near the bow in Figs. 13 and 14, it can be noted that their spray generation mechanisms were different. Longer wave 6W2 causes larger pitch motion than that of the steeper wave 6W4. In the former case, the sheet of water rose along the hull of the ship as the pitching bow encountered the wave, where in the later case, the spray formed directly at the time of splashing the wave crest. These mechanisms are elaborated in Mintu et al. (2021).

None of the zero forward speed cases generated any spray. The ship model simply rode the incoming wave in a phase similar to 2D cases. This implies that the traditional approach of simulating forward speed using the relative velocity concept may not be ideal for wave generated spray analysis since it is missing the generated wave energy from the moving vessel (Mintu et al., 2021). Fig. 15 shows a bow wave generated at forward speed in calm water and Fig. 16 shows a green water event. Such events were excluded from the calculation of the amount of spray water to isolate the spray events. Fig. 17 shows a sliced view of various phases of the water sheet development over time.

The particle resolution did not significantly affect the global spray properties. The incoming flow rate of the spray water and the ejection velocity can be seen in Fig. 18. The particle resolution only affects the local distribution of the spray water. The disintegration of water sheets into ligaments and droplets is better captured at higher resolution as can be seen in Fig. 19.

Fig. 20 shows larger wave periods cause larger pitch motions for ships traveling at the same speed. This consequently produces a larger amount of spray water. This trend is consistent with the theoretical (Mintu et al., 2021) and empirical (Zakrzewski, 1986b) models.

4.4. Multi-phase spray simulation

Multi-phase simulations with water and air particles were also conducted in a 2D environment only to demonstrate how the wind con-

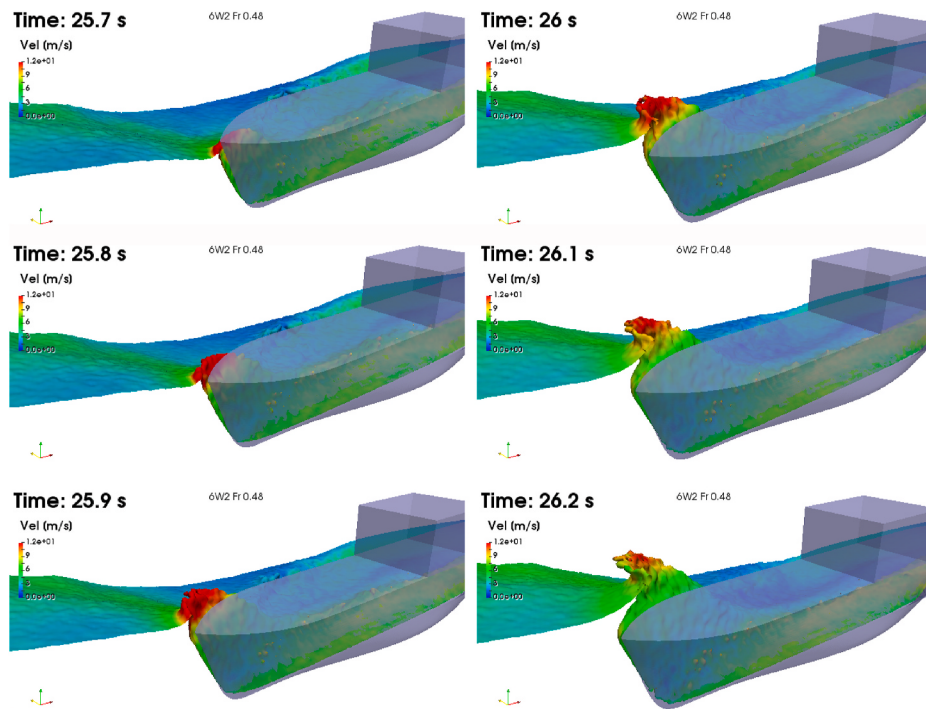


Fig. 17. Development phases of water sheet generation due to ship-wave impact. Sliced views at the centerline of the ship are shown for better visualization.

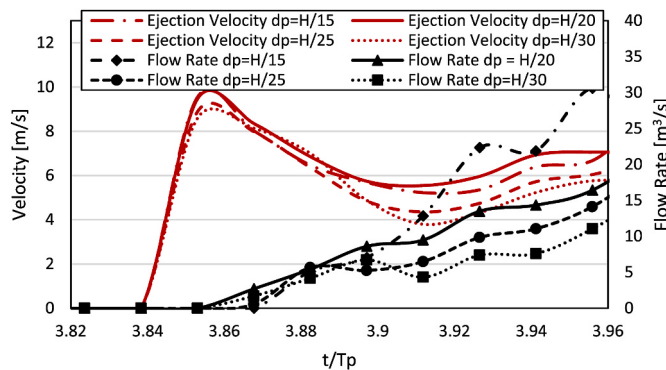


Fig. 18. Effect on particle resolution on spray properties.

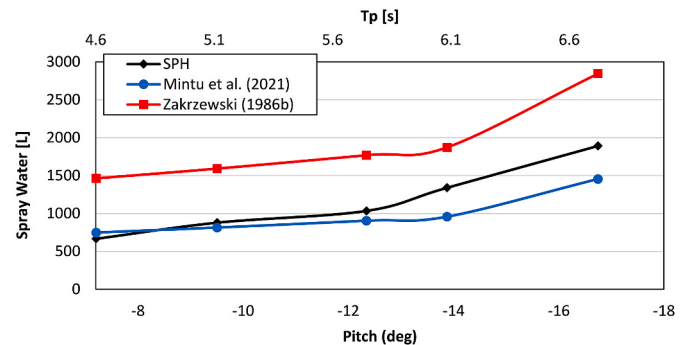


Fig. 20. Effect of wave frequency and pitch motion on the production of spray water.

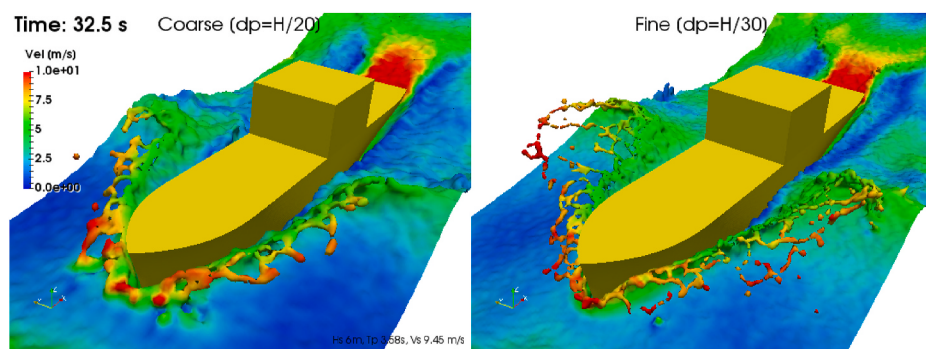


Fig. 19. Comparison of fine and coarse particle resolution of the generated spray. The left figure shows coarse spray, while the right figure captures finer details of the disintegration of water sheets into ligaments and droplets.

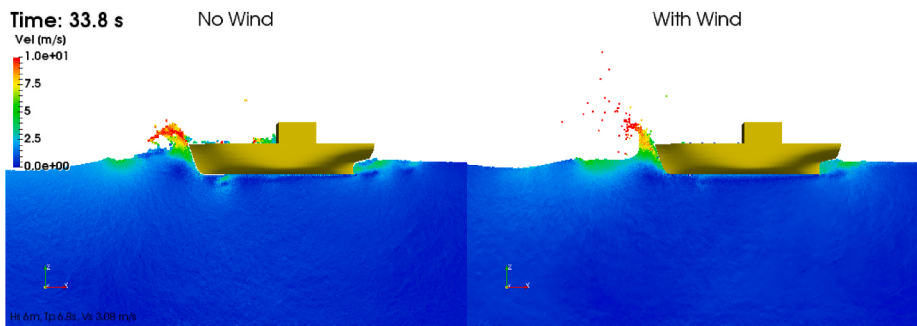


Fig. 21. Contribution of winds in fragmentation of water sheet. The left side shows a water sheet in no wind condition, and the right side shows the disintegration of the water sheet and the resultant distributions of droplets due to wind action.

tributes to the distribution of spray droplets. The same size domain with an additional layer of air particles up to 24 m high was included, giving the domain size 260 m × 60 m. A wind velocity of 11 m/s was imposed on the air particles in the direction of wave propagation in the form of a periodic boundary condition (Crespo et al., 2015). A dp resolution of $H/40$ created 710,000 particles and took 7 h to simulate 56 s of physical time. A 3D version of the same simulation would require 85 million particles and more than 7 days of run time, which is beyond the limit of the available computing resources. Fig. 21 demonstrates how wind contributes to the realistic fragmentations of water sheets into spray droplets. Future studies should explore this phenomenon as higher-performing GPUs become available.

5. Conclusions

This study develops a numerical simulation of ship-generated spray due to wave impacts using the smooth particle hydrodynamics (SPH) method both in 2D and 3D. Such novel simulations offer advantages over scale model experiments and full-scale field trials in the study of ship generated spray phenomena. A previously published field experiment of a Russian medium-size fishing vessel was used to compare with the simulation results. Representative regular waves, reported from the field data, as well as additional waves were reproduced in a deep water numerical wave basin. The basin was fitted with a flap-type wave maker and a numerical wave damper, where the fishing boat traveled at various speeds in head sea conditions. The ship was allowed to surge, heave, and pitch, while other motions were restricted. Creating the simulation “environment” for spray generation was not straightforward. Several techniques for wave generation, wave absorption, ship motion (imposed vs natural), and inlet/outlet boundary conditions were utilized and the best combinations are reported in this study.

The simulations demonstrated the development process of spray generation and its formation mechanisms. This includes the process by which the water sheet forms and disintegrates into ligaments and droplets. The amount of spray water was measured by deploying a numerical collection box above the vessel's deck and compared with the field measurements and previously published theoretical model by the authors. Special attention was given to distinguishing green water events from spray events. Overall, a good agreement was found with the available data and the theoretical model. No spray was generated for zero forward speed and lower Froude numbers in low-frequency waves. For higher Froude numbers, a significant spray cloud was formed. Ship

length to wavelength ratio is shown to play an important role. The simulations can be applied to understand the spray generation process for various types of ships and offshore structures. In addition to estimating spray water, it can be used for green water loading. The simulation also allows a time analysis of the spray generation process, which has not been possible up to now.

Using an appropriate particle resolution for a very fine spray cloud in order to capture the correct physics remains a challenge, and is beyond the current computational capabilities of GPU-accelerated or massively parallel CFD software packages (Domínguez et al., 2021). To produce an average droplet size of 3 mm in the simulation, it would require 10^{12} (10,000 billion) particles. A variable particle resolution (Vacondio et al., 2013, 2016) together with multi-GPU (Domínguez et al., 2013) implementation could have improved the situation, but neither of these was available as open-source code at the time of this research. These limitations will undoubtedly be reduced over time.

Future studies should focus on spray generation in oblique waves for different sizes and types of vessels at various headings. Irregular waves should be considered as computing resources permit. A detailed formation of fine droplets and spray clouds considering air compressibility is yet to be considered. Multi-phase simulation in 3D would be the realistic model of this problem and can be developed from this point as software and hardware capabilities are expanded.

CRediT authorship contribution statement

Shafiu Mintu: Conceptualization, Methodology, Software, Writing – original draft, Writing – review & editing. **David Molyneux:** Supervision, Recommendations. **Bruce Colbourne:** Supervision.

Declaration of competing interest

The authors declare that they have no known competing financial interests or personal relationships that could have appeared to influence the work reported in this paper.

Acknowledgments

The work described in this paper was funded by the ABS Harsh Environment Technology Center and MITACS (IT13641). The access to the GPU computing facilities was provided by Compute Canada. The authors greatly acknowledge their support.

Appendix A. Lines plan

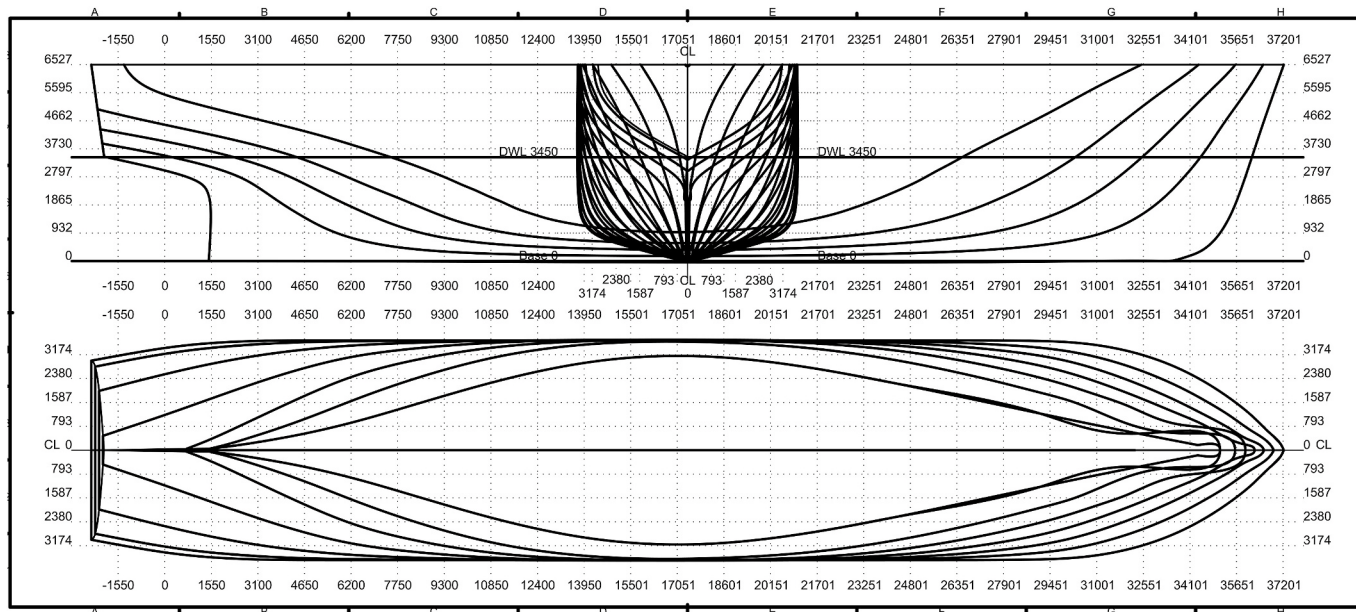


Fig. 22. Lines plan of re-created MFV Narva.

Appendix B. Supplementary data

Supplementary data to this article can be found online at <https://doi.org/10.1016/j.oceaneng.2021.110077>.

References

- Aalbers, A.B., Poen, G.J., 2015. Probabilistic modelling of marine icing: an estimation method for spray water. In: Arctic Technology Conference. <https://doi.org/10.4043/25536-MS>. St. John's, NL, Canada.
- Alkbari, H., 2019. An improved particle shifting technique for incompressible smoothed particle hydrodynamics methods. *Int. J. Numer. Methods Fluid.* 90, 603–631. <https://doi.org/10.1002/fld.4737>.
- Alkbari, H., 2018. Evaluation of incompressible and compressible SPH methods in modeling dam break flows. *Int. J. Coast. Offshore Eng.* 2, 45–57. <https://doi.org/10.29252/ijcoe.2.1.45>.
- Altomare, C., Crespo, A.J.C., Domínguez, J.M., Gómez-Gesteira, M., Suzuki, T., Verwaest, T., 2015. Applicability of Smoothed Particle Hydrodynamics for estimation of sea wave impact on coastal structures. *Coast. Eng.* 96, 1–12. <https://doi.org/10.1016/j.coastaleng.2014.11.001>.
- Altomare, C., Domínguez, J.M., Crespo, A.J.C., González-Cao, J., Suzuki, T., Gómez-Gesteira, M., Troch, P., 2017. Long-crested wave generation and absorption for SPH-based DualSPHysics model. *Coast. Eng. Coast. Eng.* 127, 37–54. <https://doi.org/10.1016/j.coastaleng.2017.06.004>.
- Altomare, C., Tafuni, A., Domínguez, J.M., Crespo, A.J.C., Gironella, X., Sospedra, J., 2020. SPH simulations of real sea waves impacting a large-scale structure. *J. Mar. Sci. Eng.* 8, 826. <https://doi.org/10.3390/jmse8100826>.
- Andreas, E.L., 1990. Time constants for the evolution of sea spray droplets. *Tellus B* 42, 481–497. <https://doi.org/10.1034/j.1600-0889.1990.t01-3-00007.x>.
- Batchelor, G.K., 1967. *An Introduction to Fluid Dynamics*. Cambridge : University Press, Cambridge.
- Begovic, E., Gatin, I., Jasak, H., Rinauro, B., 2020. CFD simulations for surf-riding occurrence assessment. *Ocean Eng.* 218 <https://doi.org/10.1016/j.oceaneng.2020.107975>.
- Bozagkhani, A., Dehghani, S.-R., Muzychka, Y.S., Colbourne, B., 2016. Understanding spray cloud formation by wave impact on marine objects. *Cold Reg. Sci. Technol.* <https://doi.org/10.1016/j.coldregions.2016.06.008>.
- Borisenkova, Y.P., Pchelko, I.G., 1975. Indicators for Forecasting Ship Icing. USACRREL Draft Transl, p. 481.
- Chung, K.K., Lozowski, E.P., Zakrzewski, W.P., Gagnon, R., Thompson, T., 1998. Spraying experiments with a model stern trawler. *J. Ship Res.* 42, 260–265.
- Crespo, A.J.C., Domínguez, J.M., Rogers, B.D., Gómez-Gesteira, M., Longshaw, S., Canelas, R.B., Vacondio, R., Barreiro, A., García-Feal, O., 2015. DualSPHysics: open-source parallel CFD solver based on smoothed particle hydrodynamics (SPH). *Comput. Phys. Commun.* 187, 204–216.
- Dalrymple, R.A., Rogers, B.D., 2006. Numerical modeling of water waves with the SPH method. *Coast. Hydron. Morphodynamics* 53, 141–147. <https://doi.org/10.1016/j.coastaleng.2005.10.004>.
- Dehghani, S.R., Muzychka, Y.S., Naterer, G.F., 2017. Water breakup phenomena in wave-impact sea spray on a vessel. *Ocean Eng.* <https://doi.org/10.1016/j.oceaneng.2017.02.013>.
- Dehghani, S.R., Muzychka, Y.S., Naterer, G.F., 2016a. Droplet trajectories of wave-impact sea spray on a marine vessel. *Cold Reg. Sci. Technol.* 127, 1–9. <https://doi.org/10.1016/j.coldregions.2016.03.010>.
- Dehghani, S.R., Naterer, G.F., Muzychka, Y.S., 2016b. Droplet size and velocity distributions of wave- impact sea spray over a marine vessel. *Cold Reg. Sci. Technol.* 132, 60–67. <https://doi.org/10.1016/j.coldregions.2016.09.013>.
- Domínguez, J.M., Crespo, A.J.C., Hall, M., Altomare, C., Wu, M., Stratigaki, V., Troch, P., Cappietti, L., Gómez-Gesteira, M., 2019. SPH simulation of floating structures with moorings. *Coast. Eng. Amst.* 153, 103560. <https://doi.org/10.1016/j.coastaleng.2019.103560>.
- Domínguez, J.M., Crespo, A.J.C., Valdez-Balderas, D., Rogers, B.D., Gómez-Gesteira, M., 2013. New multi-GPU implementation for smoothed particle hydrodynamics on heterogeneous clusters. *Comput. Phys. Commun.* 184, 1848–1860. <https://doi.org/10.1016/j.cpc.2013.03.008>.
- Domínguez, J.M., Fourtakas, G., Altomare, C., Canelas, R.B., Tafuni, A., García-Feal, O., Martínez-Estevez, I., Mokos, A., Vacondio, R., Crespo, A.J.C., Rogers, B.D., Stansby, P.K., Gómez-Gesteira, M., 2021. DualSPHysics: from fluid dynamics to multiphysics problems. *Comput. Part. Mech.* <https://doi.org/10.1007/s40571-021-00442-2>.
- Fourtakas, G., Vacondio, R., Domínguez, J., Rogers, B.D., 2020. Improved Density Diffusion Term for Long Duration Wave Propagation. Presented at the Proceedings of the International SPHERIC Workshop, Harbin, China.
- Golding, R.A., Monaghan, J.J., 1977. Smoothed particle hydrodynamics: theory and application to non-spherical stars. *Mon. Not. Roy. Astron. Soc.* 181, 375–389. <https://doi.org/10.1093/mnras/181.3.375>.
- Gómez-Gesteira, M., Rogers, B.D., Crespo, A.J.C., Dalrymple, R.A., Narayanaswamy, M., Domínguez, J.M., 2012. SPHysics – development of a free-surface fluid solver – Part 1: theory and formulations. *Comput. Geosci.* 48, 289–299. <https://doi.org/10.1016/j.cageo.2012.02.029>.
- Greco, M., Colicchio, G., Lugni, C., Faltinsen, O.M., 2013. 3D domain decomposition for violent wave- ship interactions. *Int. J. Numer. Methods Eng.* 95, 661–684. <https://doi.org/10.1002/nme.4523>.
- Horjen, I., 2013. Numerical modeling of two-dimensional sea spray icing on vessel-mounted cylinders. *Cold Reg. Sci. Technol.* 93, 20–35. <https://doi.org/10.1016/j.coldregions.2013.05.003>.

- Horjen, I., Løset, S., Vefsnmo, S., 1986. Icing Hazards on Supply Vessels and Stand-By Boats (No. N-7034). Norwegian Hydrotechnical Laboratory, Norway.
- Horjen, I., Vefsnmo, S., 1985. A Kinematic and Thermodynamic Analysis of Sea Spray (In Norwegian)., Offshore Icing — Phase II STF60 F85014 Nor. Hydrodyn. Lab. NHL Nor.
- Jones, K.F., Andreas, E.L., 2012. Sea spray concentrations and the icing of fixed offshore structures. *Q. J. R. Meteorol. Soc.* 138, 131–144. <https://doi.org/10.1002/qj.897>.
- Kanehira, T., Mutuda, H., Draycott, S., Taniguchi, N., Nakashima, T., Doi, Y., Ingram, D., 2020. Numerical re-creation of multi-directional waves in a circular basin using a particle based method. *Ocean Eng.* 209, 107446. <https://doi.org/10.1016/j.oceaneng.2020.107446>.
- Kawamura, K., Hashimoto, H., Matsuda, A., Terada, D., 2016. SPH simulation of ship behaviour in severe water-shipping situations. *Ocean Eng.* 120, 220–229. <https://doi.org/10.1016/j.oceaneng.2016.04.026>.
- Kulyakhtin, A., Tsarau, A., 2014. A time-dependent model of marine icing with application of computational fluid dynamics. *Cold Reg. Sci. Technol.* 104–105, 33–44. <https://doi.org/10.1016/j.coldregions.2014.05.001>.
- Lozowski, E.P., Szilder, K., Makkonen, L., 2000. Computer simulation of marine ice accretion. *Philos. Trans. Math. Phys. Eng. Sci.* 358, 2811–2845.
- Mintu, S., Molyneux, D., 2018. Application of GPGPU to accelerate CFD simulation. In: Proceedings of the ASME 2018 37th International Conference on Ocean, Offshore and Arctic Engineering. V002T08A001. ASME, Madrid, Spain. <https://doi.org/10.1115/OMAE2018-77649>. June 17–22, 2018.
- Mintu, S., Molyneux, D., Colbourne, B., 2021. A theoretical model for ship-wave impact generated sea spray. *J. Offshore Mech. Arctic Eng.* 143 <https://doi.org/10.1115/1.4049122>.
- Mintu, S., Molyneux, D., Oldford, D., 2016. A state-of-the-art review of research on ice accretion measurements and modelling. In: Arctic Technology Conference. St. John's, NL, Canada. <https://doi.org/10.4043/27422-MS>.
- Mintu, S.A., Molyneux, D., Colbourne, B., 2019. Multi-phase simulation of droplet trajectories of wave-impact sea spray over a vessel. In: Proceedings of the ASME 2019 38th International Conference on Ocean, Offshore and Arctic Engineering. Glasgow, Scotland, UK. <https://doi.org/10.1115/OMAE2019-95799>. V002T08A012.
- Mokos, A., Rogers, B.D., Stansby, P.K., 2016. A multi-phase particle shifting algorithm for SPH simulations of violent hydrodynamics with a large number of particles. *J. Hydraul. Res.* 1–20. <https://doi.org/10.1080/00221686.2016.1212944>.
- Mokos, A., Rogers, B.D., Stansby, P.K., Domínguez, J.M., 2015. Multi-phase SPH modelling of violent hydrodynamics on GPUs. *Comput. Phys. Commun.* 196, 304–316. <https://doi.org/10.1016/j.cpc.2015.06.020>.
- Monaghan, J.J., Cas, R.A.F., Kos, A.M., Hallworth, M., 1999. Gravity currents descending a ramp in a stratified tank. *J. Fluid Mech.* 379, 39–70. <https://doi.org/10.1017/S0022112098003280>.
- Panov, V.V., 1976. Vessel icing. *Proceeding AARI* 334, 262.
- Pereira, G.G., Cleary, P.W., Serizawa, Y., 2018. Prediction of fluid flow through and jet formation from a high pressure nozzle using Smoothed Particle Hydrodynamics. *Chem. Eng. Sci.* 178, 12–26. <https://doi.org/10.1016/j.ces.2017.12.033>.
- Roselli, R.A.R., Vernengo, G., Brizzolara, S., Guercio, R., 2019. SPH simulation of periodic wave breaking in the surf zone - a detailed fluid dynamic validation. *Ocean Eng.* 176, 20–30. <https://doi.org/10.1016/j.oceaneng.2019.02.013>.
- Ryerson, C.C., 2013. Icing Management for Coast Guard Assets (No. ERDC/CRREL TR-13-7). U.S. Army Engineer Research and Development Center, Hanover, NH.
- Ryerson, C.C., 1995. Superstructure spray and ice accretion on a large U.S. Coast Guard cutter. *Atmos. Res.* 36, 321–337. [https://doi.org/10.1016/0169-8095\(94\)00045-F](https://doi.org/10.1016/0169-8095(94)00045-F).
- Samuelson, E.M., Edvardsen, K., Graversen, R.G., 2017. Modelled and observed sea-spray icing in Arctic-Norwegian waters. *Cold Reg. Sci. Technol.* 134, 54–81. <https://doi.org/10.1016/j.coldregions.2016.11.002>.
- Sapone, D.T., 1990. A Sensitivity Study of Bow Variants on the Distribution of Sea Spray in Regular Head Seas. Massachusetts Institute of Technology, USA.
- Shadloo, M.S., Oger, G., Le Touzé, D., 2016. Smoothed particle hydrodynamics method for fluid flows, towards industrial applications: motivations, current state, and challenges. *Comput. Fluids* 136, 11–34. <https://doi.org/10.1016/j.comfluid.2016.05.029>.
- Shipilova, O., Kulyakhtin, A., Tsarau, A., Libby, B., Moslet, P.O., Løset, S., 2012. Mechanism and dynamics of marine ice accretion on vessel archetypes. In: Offshore Technology Conference. <https://doi.org/10.4043/23762-MS>. Houston, Texas, USA.
- Silva, D.F.C., Esperança, P.T.T., Coutinho, A.L.G.A., 2017. Green water loads on FPSOs exposed to beam and quartering seas, Part II: CFD simulations. *Ocean Eng.* 140, 434–452. <https://doi.org/10.1016/j.oceaneng.2016.11.008>.
- Tagliafierro, B., Mancini, S., Ropero-Giralda, P., Domínguez, J.M., Crespo, A.J.C., Viccione, G., 2021. Performance assessment of a planing hull using the smoothed particle hydrodynamics method. *J. Mar. Sci. Eng.* 9 <https://doi.org/10.3390/jmse9030244>.
- Tezdogan, T., Incevik, A., Turan, O., 2016. Full-scale unsteady RANS simulations of vertical ship motions in shallow water. *Ocean Eng.* 123, 131–145. <https://doi.org/10.1016/j.oceaneng.2016.06.047>.
- Thomas, W.L., 1991. Bering Sea Topside Icing Probabilities for Two Naval Combatants. David Taylor Research Center, Bethesda, MD.
- Vacondio, R., Rogers, B.D., Stansby, P.K., Mignosa, P., 2016. Variable resolution for SPH in three dimensions: towards optimal splitting and coalescing for dynamic adaptivity. *Comput. Methods Appl. Mech. Eng.* 300, 442–460. <https://doi.org/10.1016/j.cma.2015.11.021>.
- Vacondio, R., Rogers, B.D., Stansby, P.K., Mignosa, P., Feldman, J., 2013. Variable resolution for SPH: a dynamic particle coalescing and splitting scheme. *Comput. Methods Appl. Mech. Eng.* 256, 132–148. <https://doi.org/10.1016/j.cma.2012.12.014>.
- Veron, F., 2015. Ocean spray. *Annu. Rev. Fluid Mech.* 47, 507–538. <https://doi.org/10.1146/annurev-fluid-010814-014651>.
- Wang, Z., Yang, J., Stern, F., 2016. High-fidelity simulations of bubble, droplet and spray formation in breaking waves. <https://doi.org/10.1017/jfm.2016.87>, 792, 307, 327.
- Wang, Z.-B., Chen, R., Wang, H., Liao, Q., Zhu, X., Li, S.-Z., 2016. An overview of smoothed particle hydrodynamics for simulating multiphase flow. *Appl. Math. Model.* <https://doi.org/10.1016/j.apm.2016.06.030>.
- Zakrzewski, W.P., 1989. The use of ship icing models for forecasting icing rates on sea-going ships. In: Proceedings of the 10th International Conference on Port and Ocean Engineering under Arctic Conditions, pp. 1454–1467.
- Zakrzewski, W.P., 1986a. Icing of Fishing Vessels. Part I: Splashing a Ship with Spray. NOAA Technical Memorandum ERL PMEL-66, Seattle, Washington.
- Zakrzewski, W.P., 1986b. Splashing a ship with collision-generated spray. *Cold Reg. Sci. Technol.* 14, 65–83. [https://doi.org/10.1016/0165-232X\(87\)90045-0](https://doi.org/10.1016/0165-232X(87)90045-0).
- Zakrzewski, W.P., Lozowski, E.P., Muggeridge, D., 1988. Estimating the extent of the spraying zone on a sea-going ship. *Ocean Eng.* 15, 413–429. [https://doi.org/10.1016/0029-8018\(88\)90008-X](https://doi.org/10.1016/0029-8018(88)90008-X).
- Zha, R., Peng, H., Qiu, W., 2021. An improved higher-order moving particle semi-implicit method for simulations of two-dimensional hydroelastic slamming. *Phys. Fluids* 33, 37104. <https://doi.org/10.1063/5.0033491>, 1994.